ECS Transactions, 11 (1) 1289-1299 (2007)
10.1149/1.2781042 ©The Electrochemical Society

Durability and Activity Study of Single-Walled, Double-Walled and Multi-Walled Carbon Nanotubes Supported Pt Catalyst for PEMFCs

Zhongwei Chen[a], Weiqiao Deng[a,b], Xin Wang[a,c], Yushan Yan[a,*]

a. Department of Chemical and Environmental Engineering, and College of Engineering – Center for Environmental Research and Technology, University of California, Riverside, CA 92521
b. Division of Chemistry and Biological Chemistry, Nanyang Technological University, Singapore 637722
c. Division of Chemical & Biomolecular Engineering, Nanyang Technological University, Singapore 637722

Pt nanoparticles (2-3 nm) supported on carbon black (C), single-walled carbon nanotubes (SWNT), double-walled carbon nanotubes (DWNT) and multi-walled carbon nanotubes (MWNT) are prepared by an ethylene glycol reduction method. The catalytic activity towards the oxygen reduction reaction (ORR) and the durability of the catalysts are evaluated under condition simulating the environment of proton exchange membrane fuel cell (PEMFCs). The Pt electrochemical surface area (ECSA) of Pt/DWNT and Pt/MWNT degrade 32% after accelerated durability test (ADT), compared with 38% for Pt/SWNT and 48% for Pt/C. The degradation rate of Pt/C is about 1.5 times higher than that of Pt/DWNT. The typical ORR polarization curves of Pt/C, Pt/SWNT, Pt/DWNT and Pt/MWNT obtained before and after ADT are also examined. Before ADT, Pt/DWNT shows the highest catalytic activity towards ORR, followed by Pt/MWNT, Pt/C, and Pt/SWNT in that order. After ADT, the sequence of ORR activity of Pt/C and Pt/SWNT has changed and the overall order is: Pt/DWNT > Pt/MWNT > Pt/SWNT > Pt/C. The Pt/DWNT catalyst shows the highest catalytic activity and the best durability for ORR among the C and CNT supported Pt catalysts.

Introduction

Proton exchange membrane fuel cells (PEMFCs) are considered an attractive alternative power sources for stationary and automobile applications. The development of durable, low cost and high activity oxygen reduction reaction electrocatalysts is one of the most critical remaining challenges for the successful introduction of fuel cells into mass markets[1,2]. In state of the art PEMFCs, the most used electrocatalyst is Pt (or Pt alloys) nanoparticles supported on high surface area carbon materials. The most widely used catalyst support is carbon black such as Vulcan XC-72. Despite its widespread use, carbon black is known to undergo electrochemical oxidation to surface oxides, and eventually to CO_2 at the cathode of the fuel cell, where it is subjected to low pH, high potential, high humidity, and high temperature (~80 ^{o}C). As carbon is corroded away, noble metal nanoparticles will become loose from the electrode or aggregate to larger particles resulting in Pt surface area loss and subsequently the performance of PEMFC[1,2].

Considerable efforts have been devoted to the development of new catalyst support materials and non-supported nanostructured catalysts to improve both catalytic activity and stability[3-7]. One strategy to reduce performance degradation due to carbon corrosion is to use a more stable support. Recently, many nanostructured carbon materials[8] such as nanotubes[7,9-17], nanofibers[18,19], nanocoils[20] and nonporous hollow spheres[21,22], have been used as catalyst supports for PEMFCs. Among them, carbon nanotubes (CNTs) have been proposed as a promising support material for fuel cell catalysts due to its unique characteristics, including high aspect ratio, high electron conductivity, enhanced mass transport capability and high corrosion resistance[8]. A large amount of studies have shown that Pt (or Pt alloys)

supported on single-walled carbon nanotubes (SWNT) or multi-walled carbon nanotubes (MWNT) exhibits better performance for the electro-oxidation of methanol and oxygen reduction reaction and higher durability than that on Vulcan XC-72[12,13,23-26]. Our previous study has used double-walled carbon nanotube (DWNT) supported Pt as a high performance anode catalyst for direct methanol fuel cells (DMFCs)[27]. In this work, a systematic study of the catalytic activity towards oxygen reduction reaction (ORR) and the durability of these three types of CNTs (SWNT, DWNT and MWNT) based catalyst for PEMFCs are carried out for the first time. DWNT appear to be an ideal catalyst supports because they have higher electronic conductivity and higher thermal and chemical stability[28,29] than SWNT and in addition, and much higher surface area (500 – 1000 m^2/g) than MWNT (100 - 200 m^2/g)[28,29]. High electronic conductivity, high surface area and high corrosion resistance are the essential requirements of an electrocatalyst support.

Experimental Section

The SWNT, MWNT and DWNT were purchased from NANOCYL S.A. and they were produced via the catalytic chemical vapor deposition (CCVD) process. The diameter of the DWNT is about 3 nm (bundled at about 10 - 20 nm) and their surface area is about 600 - 1000 m^2/g. The MWNT has a diameter of 10 – 20 nm and a surface area of 300 m^2/g. The diameter of the SWNT is about 2 nm (bundled at about 10 - 20 nm) and their surface area is about 800 -1000 m^2/g. All the CNTs in the experiments were surface oxidized by a 2 M H_2SO_4 - 4 M HNO_3 mixture for 6 hours under refluxing.

Pt/CNT catalysts were prepared by an ethylene glycol (EG) reduction method. The preparation method is briefly described below using DWNT as a typical example. The surface oxidized DWNT (200 mg) was suspended in an EG solution and treated in an ultrasonic bath. Then an EG solution of hexachloroplatinic acid was added drop wise, under mechanically stirring conditions for 4 hours. A solution of 1.0 M NaOH in EG was added to adjust the pH of the synthesis solution to above 13, and then the mixture was heated at 140 ^oC for 3 hours to reduce the Pt completely. The whole process was conducted in a three-neck flask equipped with stirrer, reflux condenser and thermometer under refluxing and protected by flowing argon. After adjusting PH= 4 - 5 by 1 M HCl solution, filtration (Whatman, Grade 1), washing, and drying in a vacuum oven at 80 ^oC for 8 hours, the Pt /DWNT catalyst was obtained. The filtrated solvent was clear and the weight calculation showed the Pt conversion was nearly 100% during the deposition process. TGA analysis showed the Pt/DWNT sample had about 30 wt% Pt loading. We similarly prepared 30 wt% Pt on C, SWNT, and MWNT.

Pt/C, Pt/SWNT, Pt/MWNT and Pt/DWNT powders were characterized by X-ray diffraction (XRD) using Cu-Kα radiation with a Ni filter. The tube current was 40 mA with a tube voltage of 40 kV. The 2θ regions between 20^o to 85^o were explored at a scan rate of 5^o/min. Transmission electron microscopy (TEM) was carried out on a PHILIPS CM300 operating at 300 kV.

The electrochemical measurements were conducted in a thermostated standard electrochemical cell using a glassy carbon (GC) rotating disk electrode (RDE) setup with a multichannel potentiostats (VMP, Princeton Applied Research) and a rotation control (MSR, Pine Instruments). Potentials were determined using a Hg/Hg_2SO_4 (0.5M H_2SO_4) electrode, separated from the working electrode compartment by a closed electrolyte bridge. All potentials in this study, however, refer to that of the reversible hydrogen electrode (RHE). Fig. 1 shows the preparation method of the working electrode[30,31]. In short, aqueous suspensions of 2 $mg_{Pt}ml^{-1}$ were obtained by ultrasonic mixing for about 15 min. GC disk electrodes (5 mm diameter, 0.198 cm^2, AFE3T050GC, Pine Research Instrumentation) served as the substrate for the supported catalyst and were polished to a mirror finish (No. 40-7218 Microcloth, Buehler). An aliquot of catalyst suspension was pipetted onto the carbon substrate, leading to a metal loading of 20 μg_{Pt} cm^{-2} for Pt/C, Pt/SWNT, Pt/MWNT and Pt/DWNT. After evaporation of the water in air, 10 µl of a 0.05 wt % Nafion solution (diluted from 5 wt % Nafion®, Ion Power Inc.) was pipetted on the electrode surface in order to attach the catalyst particles onto the glassy carbon RDE, yielding a Nafion® film thickness of ca. 0.1 µm. Finally, Nafion-coated catalyst layer on the GC was soaked in DDI H_2O for 6 h before using.

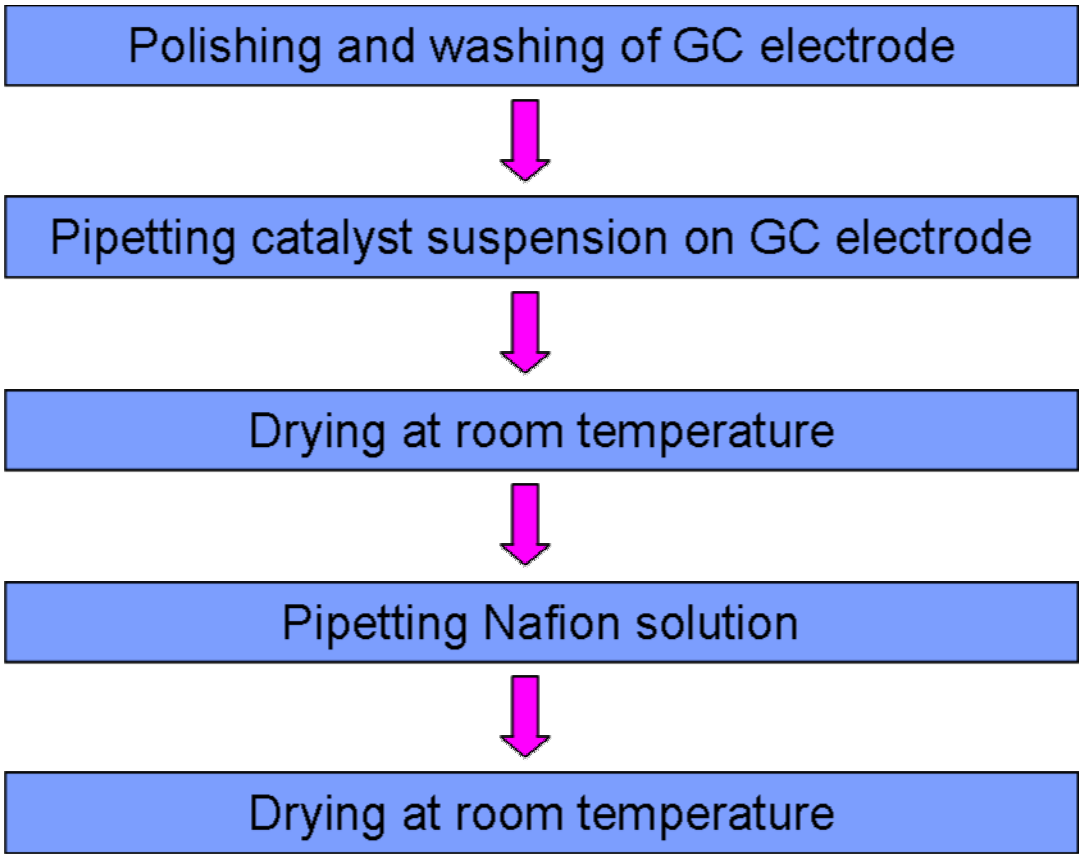

Fig 1. Preparation protocol of catalyst dispersed GC disk electrode.

The cyclic voltammetry (CV) based accelerated durability test (ADT) was performed on the working electrode by cycling the voltage between 0.05 V to 1.2 V vs RHE in an N_2 purged 0.5 M H_2SO_4 solution at room temperature. The scan rate used was 50 mV/s. The electrochemical surface areas were calculated from the H_2 desorption peak of the CV cycle. In total 1000 cycles of CV were performed for each catalyst.

The area of adsorption or desorption of atomic hydrogen on the curve of the cyclic voltammogram has been frequently used to estimate the surface area of catalysts. The cathodic and the anodic peaks appearing between 0.05 and 0.35 V versus RHE originated from H-adsorption and H-desorption in acidic media. By using the charge passed for H-desorption Q_H, electrochemical active surface area (ECSA) of platinum can be estimated by equation (1):

$$ECSA = \frac{Q_H}{m \cdot c} \qquad (1)$$

where Q_H = the charge for hydrogen desorption (mC/cm^2),

m = the Pt loading (mg/cm^2) in the electrode

c = the charge required to oxidize a monolayer of hydrogen on Pt (0.21 mC/cm^2).

For the oxygen reduction experiments the electrolyte was saturated with oxygen. The electrode potential was cycled several times between 0.05 and 1.2 V in order to produce a clean electrode surface. Current densities were normalized either to the geometric area of the glassy carbon substrate (0.198 cm^2) or the Pt surface area. The scan rate used was 5 mV/s.

The measured current density, j, is described by the following relation[32]:

$$\frac{1}{j} = \frac{1}{j_k} + \frac{1}{j_d} \quad (2)$$

Where j_k and j_d are the kinetically and diffusion-limited current densities, respectively. Then the kinetic currents were calculated based on equation (3):

$$j_k = \frac{j_d * j}{j_d - j} \quad (3)$$

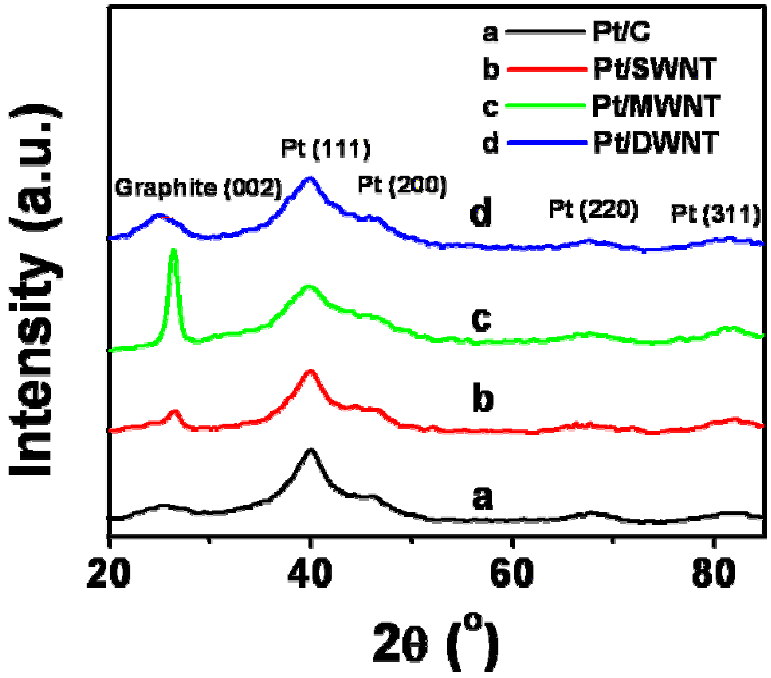

Fig 2. X-ray diffraction patterns of (a) Pt/C, (b) Pt/SWNT, (c) Pt/MWNT and (d) Pt/DWNT powder.

Results and Discussion

The XRD patterns for the Pt/C, Pt/SWNT, Pt/MWNT and Pt/DWNT samples are shown in Fig.2. The diffraction peak observed at 23-27^o is attributed to the hexagonal graphite structure (002), which can reflect the graphite degree of carbon material. Among all of the samples, MWNTs have the highest diffraction peak (002), indicating that MWNTs have the highest graphite degree, SWNT, DWNT, and C appear to have similar graphite degree. The analysis of other diffraction peaks shows that all catalysts have Pt face centered cubic (fcc) crystal structure. From the isolated Pt (220) peak, the mean particle size is about 2.4 nm, calculated with the Scherrer formula for all the Pt/C, Pt/SWNT, Pt/MWNT and Pt/DWNT samples. This is consistent with the fact that all these catalysts were prepared by the colloidal method where the Pt nanoparticles were formed before the deposition onto the support materials. Thus, the particle size of Pt on these supports is expected to be very similar.

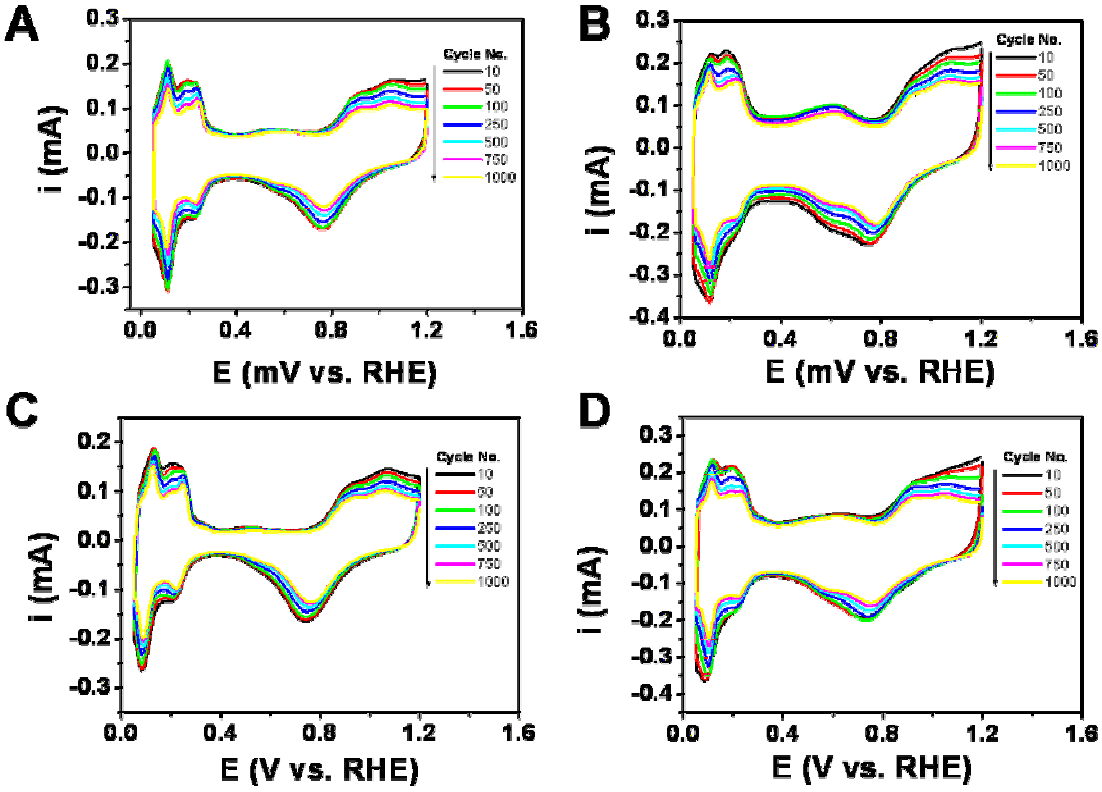

Fig 3. Cyclic voltammetry (CV) curves for (A) Pt/C, (B) Pt/SWNT, (C) Pt/MWNT and (D) Pt/DWNT catalyst in N_2 purged 0.5 M H_2SO_4 solution and 50 mV/s scan rate at different cycle numbers.

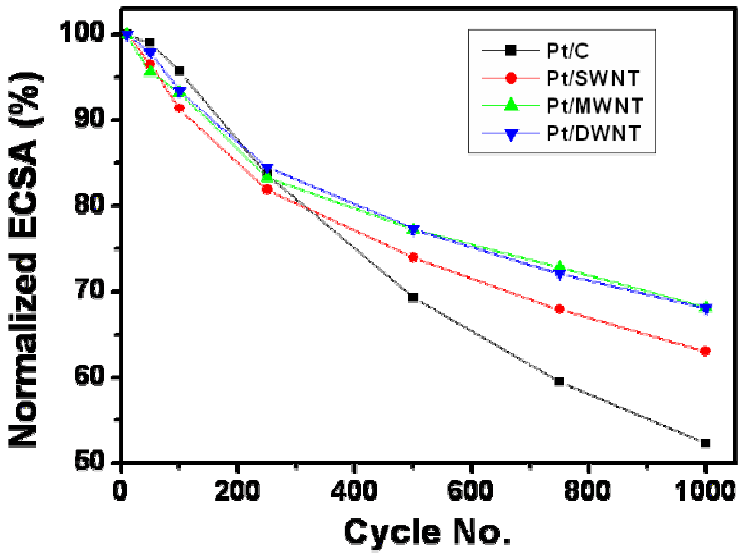

Fig 4. Comparison of Pt electrochemical surface area (ECSA) of Pt/C, Pt/SWNT, Pt/MWNT and Pt/DWNT at different number of cyclic voltammogram (CV) cycles during ADT.

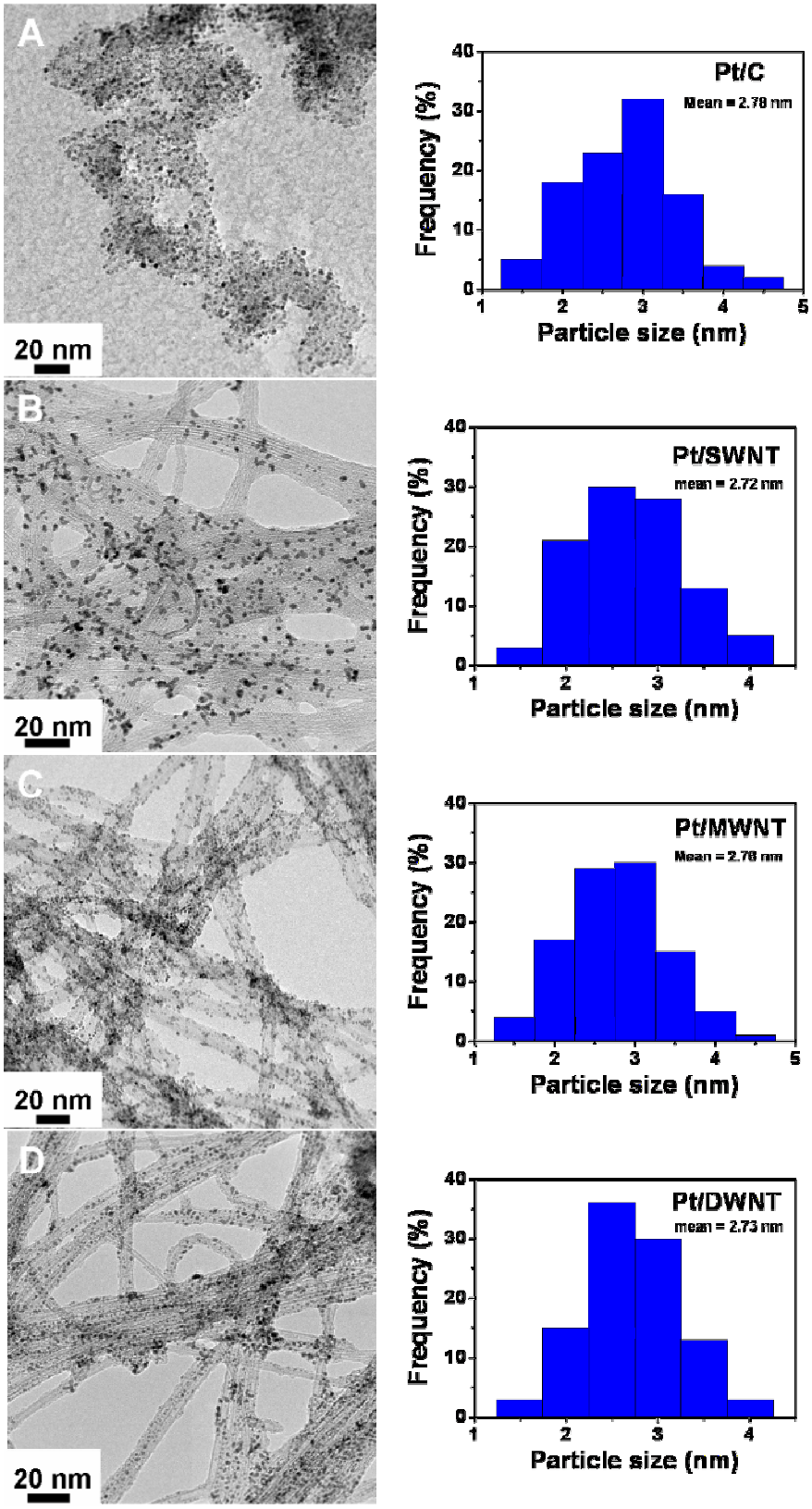

Fig 5. TEM images and particle distribution histograms of catalysts before ADT: (A) Pt/C, (B)Pt/SWNT, (C) Pt/MWNT and (D) Pt/DWNT.

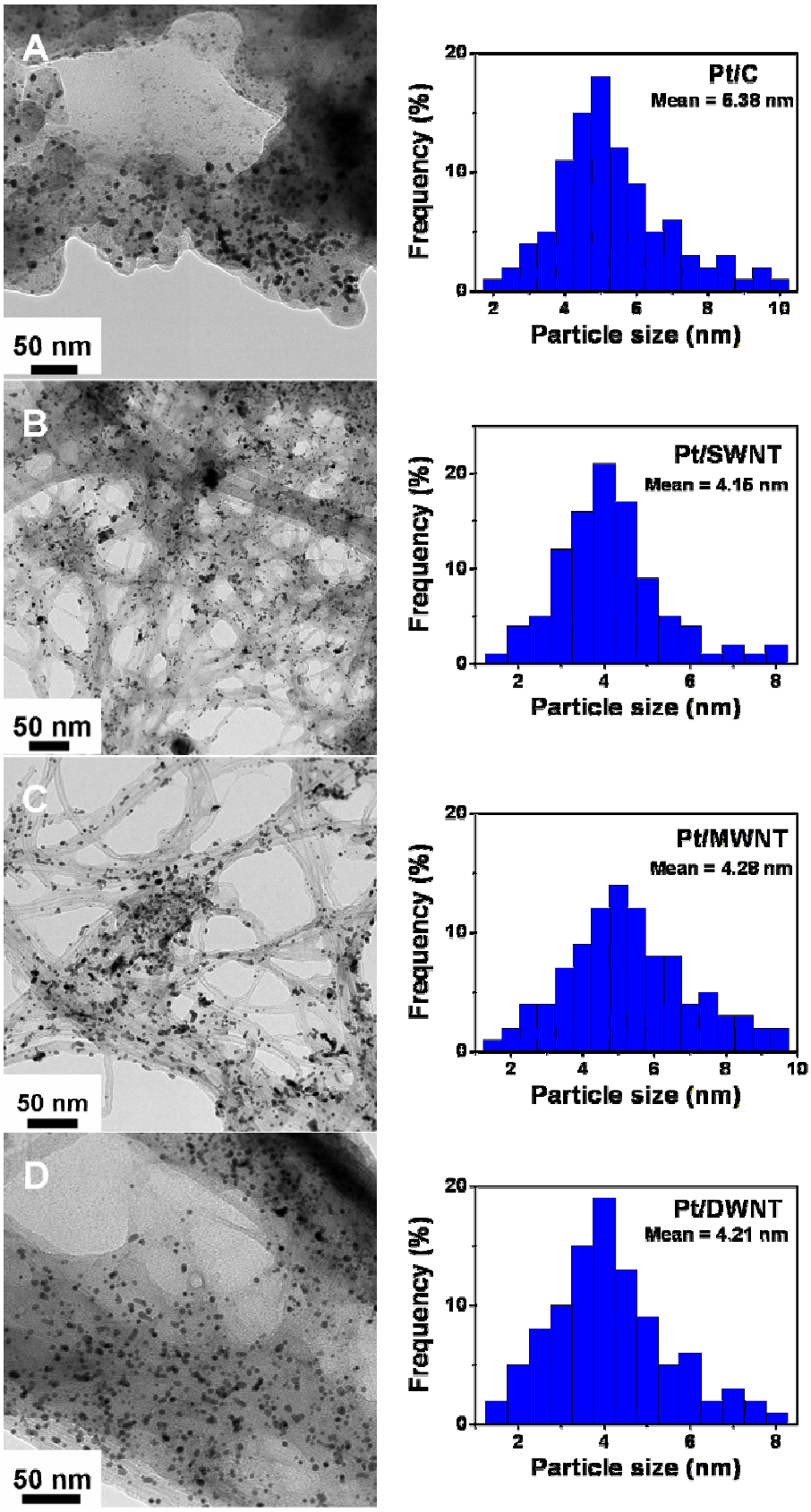

Fig 6. TEM images and particle distribution histograms of catalysts after ADT: (A) Pt/C, (B)Pt/SWNT, (C) Pt/MWNT and (D) Pt/DWNT.

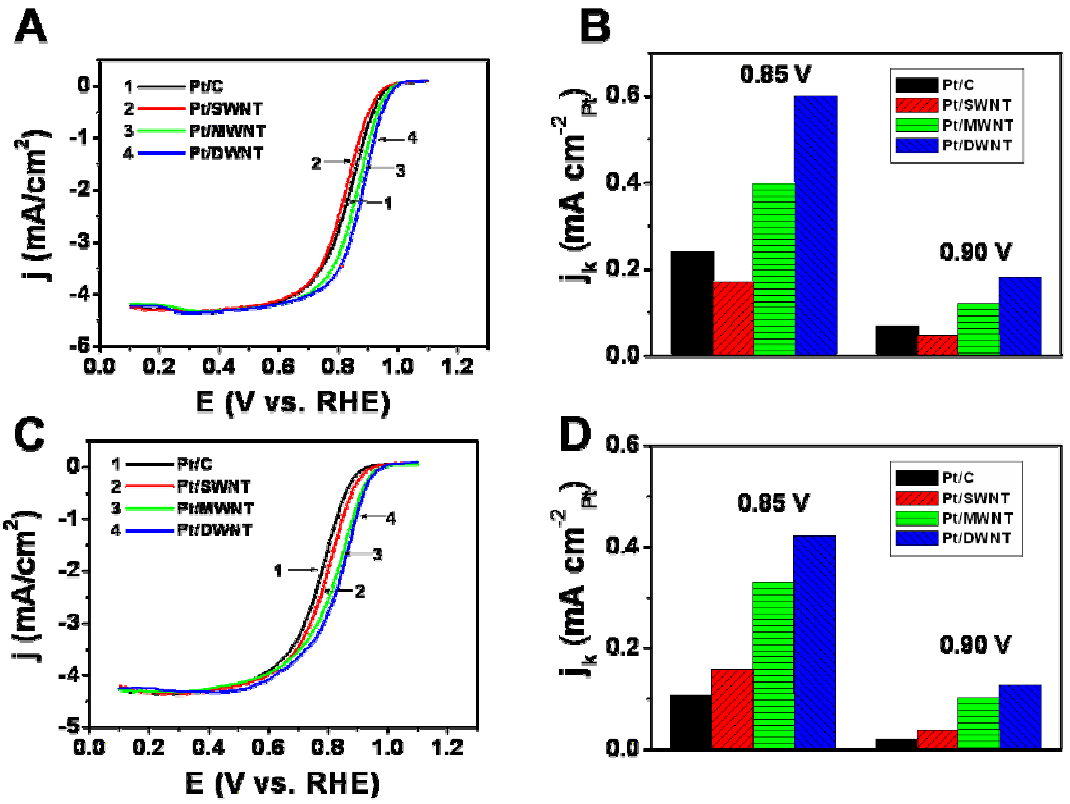

Fig 7. Polarization curves for the oxygen reduction reaction on Pt/C, Pt/SWNT, Pt/MWNT and Pt/DWNT catalysts on a rotating disk electrode, before (A) and after (C) ADT. Specific activities for the oxygen reduction reaction of Pt/C, Pt/SWNT, Pt/MWNT and Pt/DWNT catalysts before (B) and after (D) ADT.

It is generally believed that the ECSA is one of the important parameters for characterizing a fuel cell electrode. A larger ECSA means more active Pt sites are available for electrode reaction. The performance degradation of electrodes in PEMFCs is mainly due to the ECSA decrease of the electrodes. The accelerated durability tests (ADT) of an electrocatalyst can be evaluated by repeated cyclic voltammetry (CV) cycles with the proper lower and upper potential limits in an acid solution. Our ADT was conducted by cycling the electrode potential between 0.05 and 1.2 V vs. RHE at a scan rate of 50 mV/s in an N_2 purged 0.5 M H_2SO_4 solution at room temperature. Fig. 3 shows the representative cyclic voltammograms of Pt/C, Pt/SWNT, Pt/MWNT and Pt/DWNT with an increasing number of cycles during ADT. The normalized ECSA as a function of the CV cycle number obtained for Pt/C, Pt/SWNT, Pt/MWNT and Pt/DWNT is summarized in Fig. 4. The initial Pt ECSA of Pt/C, Pt/SWNT, Pt/MWNT and Pt/DWNT are similar, which are 63.5, 64.8, 64.5 and 65 m^2/g, respectively. These values are in the reasonable range as reported by others[25,31,33]. The slight ECSA difference between these catalysts may not be necessarily due to the Pt dispersion or size difference. It is most likely that the slight Pt ECSA difference is caused by the different morphologies of these supports. When the catalyst powders are dried on a glassy carbon surface to form the electrode thin film, their packings are different due to their morphology difference, which leads to the slightly different surface accessibility of Pt. The Pt ECSAs of Pt/MWNT and Pt/DWNT after ADT only decrease by 32% after 1000 cycles, followed by a 38% loss for the Pt/SWNT, and the Pt/C catalyst lost about 48% of its Pt ECSA. The Pt ECSA decrease of Pt/C is about 1.5 times higher than that of Pt/DWNT, which corresponds to the degradation rate of the catalysts: Pt/C >> Pt/SWNT > Pt/MWNT ≈ Pt/DWNT. The

degradation of ECSA can be attributed to several factors: (i) loss of Pt from the electrical contact due to the carbon support corrosion, (ii) Pt Ostwald ripening of the Pt nanoparticles, (iii) Pt nanoparticle aggregation driven by surface energy minimization, (iv) Pt nanoparticle dissolution. Here we mainly focus on the carbon support factors for the ECSA degradation. The different degradation rates of these four catalysts (Pt/C, Pt/SWNT, Pt/MWNT and Pt/DWNT) could be attributed to the different corrosion resistance of their supports and different interaction strength between the Pt nanoparticles and supports. Among these four support materials, the corrosion resistance capability rank is C << SWNT < DWNT ≤ MWNT[12,34], which corresponds to their ECSA degradations. The best corrosion resistance capability of DWNT and MWNT is the major contributor of the best durability of Pt/DWNT and Pt/MWNT among these catalysts. At the same time, the stronger interaction between CNTs and Pt nanoparticles could also reduce the Pt nanoparticles aggregation during ADT.

The Pt/C, Pt/SWNT, Pt/MWNT and Pt/DWNT catalysts before and after ADT were examined by TEM (Fig 5 and Fig. 6). Typical TEM images of the original Pt/C, Pt/SWNT, Pt/MWNT and Pt/DWNT catalysts are shown in Fig 5. Overall, small Pt nanoparticles with diameters from 2 to 3 nm and tightly grouped distributions are uniformly dispersed onto these supports. This is consistent with the XRD results. The Pt nanoparticle size in these catalysts increases greatly and the distribution becomes broader after the ADT (Fig. 6). Specifically, the Pt nanoparticles of Pt/C increase most from 2.8 nm to 5.4 nm (Fig. 5 and 6), while the Pt nanoparticles only change from 2.7 to 4.2 nm for Pt/SWNT, from 2.8 to 4.3 nm for Pt/MWNT, and from 2.7 to 4.2 nm for Pt/DWNT. These phenomena are consistent with the Pt ECSA changes of these catalysts before and after ADT. The smaller Pt particle size change in Pt ECSA Pt/SWNT, Pt/MWNT and Pt/DWNT, compared to Pt/C, could be attributed to the higher corrosion resistance of SWNT, MWNT and DWNT and the strong interaction between the Pt and CNTs.

Fig. 7 shows typical ORR polarization curves of Pt/C, Pt/SWNT, Pt/MWNT and Pt/DWNT obtained before and after ADT at room temperature in O_2 saturated 0.5 M H_2SO_4 using a rotating disk electrode (RDE) at 1600 rpm. A RDE test can provide the specific activity of the catalysts in a well-controlled environment without mass transportation effects. The half-wave potentials of Pt/C, Pt/SWNT, Pt/MWNT and Pt/DWNT are 831, 824, 864 and 871 mV, respectively, showing that the catalytic activity sequence towards ORR is Pt/DWNT > Pt/MWNT > Pt/C > Pt/SWNT. Fig. 7B shows the specific activity of these catalysts, which is a better indicator of electrocatalyst quality. Pt/DWNT has the highest specific activity (0.599 mA/cm^2_{Pt}) at 0.85 V, 1.5 times that of Pt/MWNT (0.398 mA/cm^2_{Pt}), 2.5 times of Pt/C (0.239 mA/cm^2_{Pt}), and 3.5 times of the Pt/SWNT (0.171 mA/cm^2_{Pt}). The remarkably high catalytic activity of Pt/DWNT is not fully understood. Some favorable factors such as high electrical conductivity, high surface area and porosity of the support are involved in determining the overall catalytic activity. The small diameter of the DWNT may have lead to a unique interaction between Pt and the DWNT that facilitates charge transfer from Pt to the tubes, and improving the specific activity of Pt. The bundle morphology of the DWNTs may also help the uniform distribution of porosity and Nafion in the thin film electrode, further improving the Pt mass activity. Although the Pt ECSA decreases during ADT, there is no change in the limiting currents. It is believed that at the high voltage bias used, the reaction kinetics is so fast that the process is still diffusion limited even after some significant reduction of Pt ECSA in the electrode. On the other hand, the half-wave potentials of Pt/C, Pt/SWNT, Pt/MWNT and Pt/DWNT decreased to 773, 788, 829 and 837 mV after ADT. The catalytic activity sequence towards ORR of Pt/C and Pt/SWNT were changed before and after ADT. After ADT, the order is: Pt/DWNT > Pt/MWNT > Pt/SWNT > Pt/C. The Pt/DWNT showed the smallest degradation (34 mV). In contrast, the corresponding half-wave potential change for Pt/C amounts to a loss of 58 mV. When comparing the specific activities of these catalysts after ADT, Pt/DWNT still has the highest specific activity (0.421 mA/cm^2_{Pt}) at 0.85 V, followed by Pt/MWNT (0.331 mA/cm^2_{Pt}), while the specific activity of Pt/SWNT (0.157 mA/cm^2_{Pt}) became higher than that of Pt/C (0.107 mA/cm^2_{Pt}) and the ratio of specific activity of Pt/DWNT to Pt/C has been enlarged from 2.5 times to 3.9 times. As expected, the ORR catalytic activity measurements are in good agreement with the measured ECSA. Table 1 gives a summary of the observed changes in surface area and catalytic activity data caused by ADT. These ADT experiments suggest that DWNT is a superior support to

anchor Pt particles. In addition to the improved catalytic activity, the DWNT support minimizes the Pt aggregation effect during long-term usage.

Table 1. A comparison of surface area and catalytic activity data for Pt/C, Pt/SWNT, Pt/MWNT and Pt/DWNT before and after ADT.

Catalyst	Pt dispersion (m^2/gPt)		Half-wave potential (V)		Specific kinetic current density at 0.85 V (mA/cm^2 Pt)	
	initial	*after-ADT*	*initial*	*after-ADT*	*initial*	*after-ADT*
Pt/C	63.5	33.2	0.831	0.773	0.239	0.107
Pt/SWNT	64.8	40.8	0.824	0.788	0.171	0.157
Pt/MWNT	64.5	43.9	0.864	0.829	0.398	0.331
Pt/DWNT	65.0	44.2	0.871	0.837	0.599	0.421

Conclusions

In summary, C, SWNT, MWNT and DWNT supported highly dispersed Pt nanoparticles with small and uniform particle size have been prepared successfully by the EG reduction method. The catalytic activity towards oxygen reduction reaction and the stability of Pt/C, Pt/SWNT, Pt/MWNT and Pt/DWNT have been evaluated using a thin film rotating disk electrode under simulated PEMFC conditions. Pt/DWNT exhibited the best catalytic activity towards ORR. It is also evident from the accelerated durability tests that DWNT enhances the stability of the electrocatalyst greatly. Therefore, the DWNT is a promising support candidate for improving the catalytic activity and durability performance of electrocatalysts in PEMFCs.

Acknowledgements

This work was financially supported by the Department of Energy, Pacific Fuel Cell Corp., and UC-Discovery Grant. We thank Dr. Y. M. Tsou of E-TEK for helpful discussion.

References

1. Xie, J.; Wood, D. L.; Wayne, D. M.; Zawodzinski, T. A.; Atanassov, P.; Borup, R. L. *Journal of the Electrochemical Society* **2005**, *152*, A104-a113.
2. Knights, S. D.; Colbow, K. M.; St-Pierre, J.; Wilkinson, D. P. *Journal of Power Sources* **2004**, *127*, 127-134.
3. Chen, Z. W.; Li, W. Z.; Waje, M.; Yan, Y. S. *Angewandte Chemie, International Edition* **2007**, *46*, 4060-4063.
4. Chen, Z. W.; Xu, L. B.; Li, W. Z.; Waje, M.; Yan, Y. S. *Nanotechnology* **2006**, *17*, 5254-5259.
5. Bashyam, R.; Zelenay, P. *Nature* **2006**, *443*, 63-66.
6. Eikerling, M.; Ioselevich, A. S.; Kornyshev, A. A. *Fuel Cells* **2004**, *4*, 131-140.
7. Wang, C.; Waje, M.; Wang, X.; Tang, J. M.; Haddon, R. C.; Yan, Y. S. *Nano Letters* **2004**, *4*, 345-348.

8. Lee, K.; Zhang, J. J.; Wang, H. J.; Wilkinson, D. P. *Journal of Applied Electrochemistry* **2006**, *36*, 507-522.
9. Li, W. Z.; Liang, C. H.; Zhou, W. J.; Qiu, J. S.; Zhou, Z. H.; Sun, G. Q.; Xin, Q. *Journal of Physical Chemistry B* **2003**, *107*, 6292-6299.
10. Li, W. Z.; Wang, X.; Chen, Z. W.; Waje, M.; Yan, Y. S. *Langmuir* **2005**, *21*, 9386-9389.
11. Waje, M. M.; Wang, X.; Li, W. Z.; Yan, Y. S. *Nanotechnology* **2005**, *16*, S395-S400.
12. Wang, X.; Li, W. Z.; Chen, Z. W.; Waje, M.; Yan, Y. S. *Journal of Power Sources* **2006**, *158*, 154-159.
13. Girishkumar, G.; Vinodgopal, K.; Kamat, P. V. *Journal of Physical Chemistry B* **2004**, *108*, 19960-19966.
14. Xing, Y. C. *Journal of Physical Chemistry B* **2004**, *108*, 19255-19259.
15. Kim, C.; Kim, Y. J.; Kim, Y. A.; Yanagisawa, T.; Park, K. C.; Endo, M.; Dresselhaus, M. S. *Journal of Applied Physics* **2004**, *96*, 5903-5905.
16. Yuan, F. L.; Ryu, H. J. *Nanotechnology* **2004**, *15*, S596-S602.
17. Matsumoto, T.; Komatsu, T.; Arai, K.; Yamazaki, T.; Kijima, M.; Shimizu, H.; Takasawa, Y.; Nakamura, J. *Chemical Communications* **2004**, 840-841.
18. Steigerwalt, E. S.; Deluga, G. A.; Lukehart, C. M. *Journal of Physical Chemistry B* **2002**, *106*, 760-766.
19. Bessel, C. A.; Laubernds, K.; Rodriguez, N. M.; Baker, R. T. K. *Journal of Physical Chemistry B* **2001**, *105*, 1115-1118.
20. Park, K. W.; Sung, Y. E.; Han, S.; Yun, Y.; Hyeon, T. *Journal of Physical Chemistry B* **2004**, *108*, 939-944.
21. Joo, S. H.; Choi, S. J.; Oh, I.; Kwak, J.; Liu, Z.; Terasaki, O.; Ryoo, R. *Nature* **2001**, *412*, 169-172.
22. Yu, J. S.; Kang, S.; Yoon, S. B.; Chai, G. *Journal of the American Chemical Society* **2002**, *124*, 9382-9383.
23. Girishkumar, G.; Hall, T. D.; Vinodgopal, K.; Kamat, P. V. *Journal of Physical Chemistry B* **2006**, *110*, 107-114.
24. Girishkumar, G.; Rettker, M.; Underhile, R.; Binz, D.; Vinodgopal, K.; McGinn, P.; Kamat, P. *Langmuir* **2005**, *21*, 8487-8494.
25. Kongkanand, A.; Kuwabata, S.; Girishkumar, G.; Kamat, P. *Langmuir* **2006**, *22*, 2392-2396.
26. Li, L.; Xing, Y. C. *Journal of the Electrochemical Society* **2006**, *153*, A1823-A1828.
27. Li, W. Z.; Wang, X.; Chen, Z. W.; Waje, M.; Yan, Y. S. *Journal of Physical Chemistry B* **2006**, *110*, 15353-15358.
28. Endo, M.; Muramatsu, H.; Hayashi, T.; Kim, Y. A.; Terrones, M.; Dresselhaus, N. S. *Nature* **2005**, *433*, 476-476.
29. Kavan, L.; Dunsch, L.; Kataura, H. *Carbon* **2004**, *42*, 1011-1019.
30. Paulus, U. A.; Schmidt, T. J.; Gasteiger, H. A.; Behm, R. J. *J. of Electroana. Chem.* **2001**, *495*, 134-145.
31. Ferreira, P. J.; la O', G. J.; Shao-Horn, Y.; Morgan, D.; Makharia, R.; Kocha, S.; Gasteiger, H. A. *Journal of the Electrochemical Society* **2005**, *152*, A2256-a2271.
32. Shao, M. H.; Sasaki, K.; Adzic, R. R. *Journal of the American Chemical Society* **2006**, *128*, 3526-3527.
33. Liu, Z. L.; Lee, J. Y.; Chen, W. X.; Han, M.; Gan, L. M. *Langmuir* **2004**, *20*, 181-187.
34. Liu, Q. F.; Ren, W. C.; Li, F.; Cong, H. T.; Cheng, H. M. *Journal of Physical Chemistry C* **2007**, *111*, 5006-5013.